Bainite plate thickness reduction and microstructure tailoring by double austempering of Al-rich 3Mn steel

Skowronek, Adam; Cordova-Tapia, Erick; Tobajas-Balsera, Pilar; Garcia-Mateo, Carlos; Jiménez, José A.; Petrov, Roumen; Grajcar, Adam

DOI
10.1016/j.msea.2022.143743

Publication date
2022

Document Version
Final published version

Published in
Materials Science and Engineering A

Materials Science & Engineering A 853 (2022) 143743

Contents lists available at ScienceDirect

Materials Science & Engineering A

journal homepage: www.elsevier.com/locate/msea

Bainite plate thickness reduction and microstructure tailoring by double austempering of Al-rich 3Mn steel

Adam Skowronek [a], Erick Cordova-Tapia [b], Pilar Tobajas-Balsera [b], Carlos Garcia-Mateo [b], José A. Jiménez [b], Roumen Petrov [c,d], Adam Grajcar [a,*]

[a] Silesian University of Technology, Faculty of Mechanical Engineering, Department of Engineering Materials and Biomaterials, 18a Konarskiego Street, 44-100, Gliwice, Poland
[b] National Center for Metallurgical Research, Av. De Gregorio del Amo 8, Madrid, 28040, Spain
[c] Ghent University, Department of Electromechanical, Systems and Metal Engineering, Research group Materials Science and Technology, Tech Lane Ghent Science Park-Campus A Zwijnaarde, Technologiepark 46, 9052, Ghent, Belgium
[d] Delft University of Technology, Department of Materials Science and Engineering, 3mE-TUDelft, Building 34, Mekelweg 2, 2628 CD, Delft, the Netherlands

ARTICLE INFO

Keywords:
Double austempering
Bainitic transformation
Plate thickness reduction
Microstructure tailoring
Medium-Mn steels
Strength improvement
Retained austenite morphology

ABSTRACT

The novel use of double austempering treatments in a multiphase steel to refine and homogenize the final microstructure and thus improve the material strength have been studied in the 3.3Mn-0.17C-1.6Al-0.23Mo-0.22Si alloy. The microstructural features developed after conventional isothermal austempering treatments at 450 °C and 400 °C were compared with those obtained after two-step heat treatments. These treatments consisted of a first isothermal holding at a temperature slightly above the initial M_s, that was interrupted at 25 and 50% of transformation, followed by a second stage treatment at a lower temperature to complete the bainitic transformation. One- and two-step treatments were performed in a high-resolution dilatometer, and the critical transformation temperatures and phase transformation kinetics were determined from the longitudinal changes recorded during these tests. It was shown that blocky-type austenite was almost completely eliminated after the two-step treatments, which in turn positively reduced the amount of fresh martensite from ~6 to «1%. It was possible to keep the volume fraction of retained austenite above 10%, while reducing both the thickness of the bainitic plates and the film-like retained austenite by 20% and more than 40%, respectively. These microstructural characteristics made it possible to increase the hardness of the alloy by approximately 50 HV and yield strength by 180 MPa.

1. Introduction

Reduction of the thickness of the bainitic plate is crucial to obtain improved mechanical properties of austempered steels, such as hardness and toughness [1]. The final thickness of the bainitic plate is mainly determined by factors such as yield strength and dislocation density of austenite, which limit the growth of the bainitic plate (resistance to interface motion), prior austenite grain size and the driving force of transformation (increased nucleation rate) [2,3]. All of them are controlled by chemical composition and temperature of austempering [4]. In general, the thickness of the bainite plate can be refined by carrying out the bainitic transformation at lower temperatures. The temperature cannot be reduced to much as the austempering region is limited by the start temperatures of bainitic (B_s) and martensitic (M_s) transformations. The most common approach to simultaneously reduce the B_s and M_s temperatures is to increase the mean carbon concentration in the bulk material. However, a high content of this element leads to lower toughness [5] and causes weldability problems [6,7]. On the other hand, the disadvantage of using a low-temperature bainite transformation temperature is the very long holding times needed to complete the process.

Bainitic steels present two basic morphologies of austenite: carbon-enriched nanometric films located between individual plates of bainitic ferrite, and coarser blocks in between unparallel bainitic sheaves and on grain boundaries [8]. The blocky grains in general show much lower thermal and mechanical stability as compared to the thin films

* Corresponding author.
E-mail addresses: adam.skowronek@polsl.pl (A. Skowronek), erick@cenim.csic.es (E. Cordova-Tapia), mdp.tobajas@alumnos.upm.es (P. Tobajas-Balsera), c.g.mateo@csic.es (C. Garcia-Mateo), jimenez@cenim.csic.es (J.A. Jiménez), roumen.petrov@ugent.be (R. Petrov), adam.grajcar@polsl.pl (A. Grajcar).

https://doi.org/10.1016/j.msea.2022.143743
Received 21 July 2022; Received in revised form 2 August 2022; Accepted 4 August 2022
Available online 10 August 2022

due to its lower carbon concentration, and tend to transform to martensite upon cooling after the bainitic heat treatment or after a small amount of plastic deformation [9,10]. The presence of hard and brittle martensite can diminish the overall properties of the steel [11]. Sugimoto et al. [12] reported that martensitic transformation of blocky RA grains during hole-punching of steel sheets deteriorates the stretch-flangeability. Hase et al. [13] showed that ductility properties and fracture toughness were improved by eliminating blocky-type austenite. Thus, additional arguments to reduce the bainite transformation temperature are an increase in the proportion of filmy retained austenite compared to blocky morphology [21] and an improvement in its stability due to the higher carbon concentration. Due to the enhanced stability and small size, film-like RA has much better input to the mechanical properties [14]. The work of Kim et al. [15] indicates that a change of the blocky morphology of austenite to film-like one increases formability of sheet edges in punching processes.

The austempering process below the M_s temperature has been also investigated to reduce the thickness of bainitic plates and additionally accelerate the bainitic transformation [4,16,17]. The formation of martensite prior to bainite simultaneously increases the number of nucleation sites and the strength of the austenite, resulting in finer bainitic plates. Furthermore, a lower isothermal holding temperature causes a higher driving force, which also influences the thickness of the bainite that is produced. However, the martensite formed prior to isothermal holding tends to be coarse [4,18], which can lead to weakening of the structure. Tian et al. [4] showed the downward trend in properties along with a decrease in the austempering temperature below M_s due to the increasing fraction and size of the tempered martensite.

Recent efforts by some scientists have been directed towards applying double or multi-austempering treatment to refine the final microstructure. These treatments consisted of a first austempering step at a temperature above the initial bulk M_s, followed by the decomposition of carbon-enriched austenite to bainite at a lower transformation temperature in every next stage of austempering. Soliman et al. [19] have shown that two-stage austenitic quenching leads to significant refinement of bainitic plates and more stable retained austenite and thus increased strength properties of a 0.26 wt% C steel. Wang et al. [8] and Mousalou et al. [20] reported that multi-step isothermal treatment is a useful method to decrease the thickness of bainitic plates and lower the amount of austenite blocks in medium carbon TRIP-aided bainitic steels. They reported that this microstructure is accompanied by mechanical properties superior to those obtained after a conventional bainitic transformation.

However, there is no comprehensive analysis of the impact of double- or multi-austempering treatments on the microstructure – properties relationship of the latest generation of AHSS steels. Until now, research on these treatments has focused on conventional TRIP-aided steels containing Si and a carbon content greater than 0.25 wt% [8, 19–22]. This combination allows for austempering at very low temperatures, but at the cost of poor weldability [6], deteriorated galvanization ability [23] and long process time. In this work, the double austempering is applied as a novel approach to the Al-rich 3.3 Mn steel. Medium-Mn steels generally contain less than 0.2 wt% of carbon [24], while their higher concentration of Mn guarantees additional stabilization of the retained austenite and a decrease in the M_s temperature. On the other hand, replacement of Si by Al can be used simultaneously to prevent cementite precipitation and accelerate bainitic transformation [23,25]. Such chemical composition design allows to avoid the technological problems mentioned earlier, so properly heat-treated 3–5% Mn steels are an excellent candidate for high-strength automotive components. The aim of the work is to clarify the susceptibility of these Al-rich 3Mn steel to double austempering and investigate the possibility to refine and modify the microstructure morphology, improve the stabilization of RA, and finally improve the mechanical properties by the proposed method in comparison to conventional single heat-treated steels.

2. Material and methods

2.1. Material and processing variants selection

A 3.3 wt% Mn, 0.17 wt% C, 1.6 wt% Al, 0.23 wt% Mo and 0.22 wt% Si steel has been used for the investigation. The carbon concentration is maintained at a relatively low level to improve the weldability, and the RA stability is supported by increased Mn addition. After casting, the material was subjected to a thermomechanical processing consisting of forging in the temperature range of 1200 °C–900 °C followed by hot rolling in 5 passes at temperatures ranging from 1100 °C to 750 °C to obtain the final strip with a thickness of 4.5 mm. Cylindrical samples with 4 mm diameter and 10 mm length were cut from the final sheet along the rolling direction for the dilatometric investigations. The heat treatments have been conducted using a BAHR DIL 805 A/D dilatometer. This equipment uses an induction coil for heating, helium for cooling while the temperature is controlled by a K-type thermocouple welded to the central part of the sample. The longitudinal length changes were measured via a Linear Variable Differential Transducer (LVDT), using fused silica pushrods. The dilatometry data was analyzed according to ASTM A1033-04 [26]. The beginning of the phase transformation was determined as the point where the dilatation curve deviates from the straight line [27].

All heat treatments started with a first austenitization step at 1100 °C for 5 min. After austenitization, a sample was quenched at a cooling rate of 60 °C/s and from this test the bulk M_s was determined as 434 °C (Fig. 1). The first austempering at 450 °C was performed to record the bainitic transformation kinetics slightly above M_s (Fig. 1). The bainite formation results is the sample expansion – an increase in relative change in length (RCL) in dilatometric diagrams. When the dilatometric curve reaches the plateau, the transformation is considered as completed [28] and the recorded sample expansion is considered as 100% of possible bainitic transformation at a given temperature. However, it is not equivalent to transformation of 100% austenite. The bainitic transformation in steels containing Si and/or Al is accompanied by carbon diffusion from newly formed bainite to remaining austenite. When the austenite reaches some certain level of carbon enrichment the transformation is stopped, as the austenite is too stable for further transformation. By dilatometric measurement it was concluded that after 10 min the transformation at 450 °C reached this point. Based on the results, the single isothermal austempering treatments for 10 min have been performed at a temperature slightly above and another below the initial bulk M_s (450 and 400 °C, respectively). The samples developed after these reference treatments were called: 450C and 400C. The first austempering allowed to calculate the sample expansion related to complete transformation at 450 °C. Hence, the times related to the given

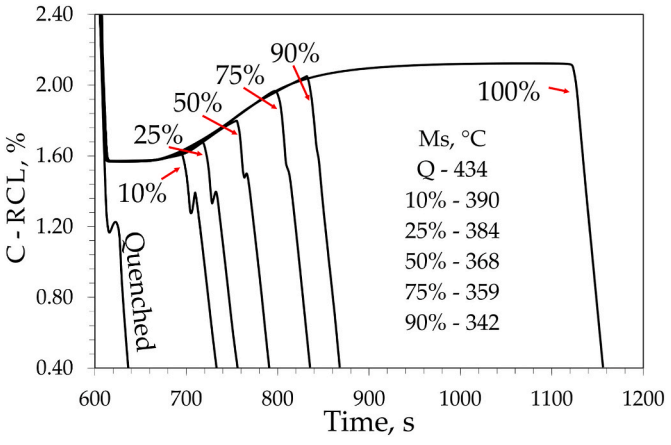

Fig. 1. M_s changes with increasing degree of bainitic transformation at 450 °C; RCL - relative change in length.

% of transformation (% of the sample expansion during the complete transformation) were computable. To record the changes in austenite stability (M_s temperature), several heat treatments (Fig. 1) were performed at a given % of transformation completion, followed by cooling to room temperature at the rate of 60 °C/s. It was concluded that 25 and 50% of bainitic transformation at 450 °C (which takes 105 and 140 s respectively), provides sufficient reduction in M_s temperature (Fig. 1) for the second austempering step. As shown in Fig. 2, double austempering treatments consisted of a first austempering step at 450 °C until the transformation of 25 or 50% of the austenite, followed by an isothermal treatment at 400 °C until completing 10 min of total treatment (samples called: 25dbl and 50dbl, respectively). The cooling rate to the austempering temperature (or to the first step of the treatments) was 60 °C/s for all samples, to the second austempering step was 10 °C/s, and final cooling rate to room temperature after the treatments (RT) was 1 °C/s.

2.2. Microstructure characterization

After dilatometric tests, metallographic samples were cut perpendicular to the length and prepared using standard procedures that involved grinding with SiC papers up to 2000 grit, polishing with 3 and 1 μm diamond paste, and a final step that included a triple etching (nital) and polishing cycle before polishing with colloidal silica suspension (0.04 μm) for 20 min. This process ensured both a free-deformation surface and a sharp definition of the different microstructural constituents after etching with Nital or Klemm's solutions. Observation of the microstructural features was performed using light (LM) and scanning electron microscopy (SEM) using Zeiss AxioObserver and a FEG-SEM, JEOL Ltd microscopes, respectively.

The volume fraction of RA was determined from the X-ray diffraction patterns recorded with Co-Kα radiation in a Bruker D8 Advance diffractometer working at 40 KV and 30 mA and equipped with a Goebel mirror and a LynxEye Linear Position Sensitive Detector. Conventional θ–2θ scans were performed over a 2θ range of 45–135° with a step size of 0.01°. The diffraction patterns were refined using the 4.2 version of the TOPAS Rietveld analysis program (Bruker AXS) and the crystallographic information of bainite and austenite for phase quantification, as well as for the determination of lattice parameter α_γ. For this analysis, the instrumental functions were empirically parameterized using the diffraction pattern of a corundum sample. Based on the lattice parameter, the carbon concentration in austenite has been calculated following the equation [28]:

$$\alpha_\gamma = 3.556 + 0.0453x_C + 0.00095x_{Mn} + 0.0056x_{Al} \quad (1)$$

Where α_γ is in Å, x_C, x_{Mn} and x_{Al} are elements concentration in austenite (wt.%)

The electron backscatter diffraction (EBSD) technique was employed to obtain additional aspects of the microstructure. The samples used for this study were slightly etched using nital (<1 s) to generate a minimal relief of the surface to navigate along the microstructure, although this may slightly decrease the scan quality. The EBSD system was attached to a FEI Quanta FEG 450 SEM with field emission gun (FEG) filament. EBSD patterns were acquired at 20 kV accelerating voltage on the sample tilted 70° from the horizontal and a probe current of ~2.5 nA using a hexagonal scan grid with 60 nm spacing. At least three areas of 40 × 40 μm^2 were analyzed for each sample. The EBSD data obtained were processed using the OIM TSL data Analysis software v. 7.3.1. A two-step clean-up procedure was performed to remove the bad data point. For the first step, a grain confidence index (CI) standardization procedure was applied employing a grain tolerance angle of 5° and a minimum grain size greater than 2 pixels [29]. A second step was neighbour orientation correlation procedure which was applied using min CI = 0.1 and clean up level 3. Finally, all points with CI ≤ 0.1 have been removed from the orientation imaging microscopy (OIM) maps before the quantification procedures of the phases and the microstructural constituents. As the fresh martensite contains higher density of lattice imperfections than bainite, it will present Kikuchi patterns, resulting in a lower image quality (IQ) [30,31]. Thus, in the color-coded phase maps, pixels characterized by a lower IQ averaged over the area of pre-defined grains were assigned to this phase.

The apparent bainite plate (BPT) and film-like retained austenite (F-RAT) thickness were identified and quantified on the obtained high-resolution SEM images using ImageJ software. The following procedure established by Garcia-Mateo et al. [32] was used according to which at least 300 linear intersections were measured for different areas of each sample to determine the mean lineal intercept $\bar{L}_T$. This value was corrected to obtain the thickness, t, using the following relation [33]:

$$\bar{L}_T = \frac{\pi t}{2} \quad (2)$$

2.3. Mechanical properties characterization

The mechanical properties were investigated using hardness and uniaxial tensile tests. The Vickers' hardness was measured using a microhardness tester FB-700 at a load of 9.81 N. Ten measurements for each sample were taken. Max and min values were excluded and the average hardness was calculated from the remaining 8 values. The uniaxial tensile tests were performed using ZWICK Z020 testing machine at a strain rate of 10^{-3} s^{-1}. The tensile samples with a gauge length of 10 mm and the cross-sectional dimensions of 3 × 3 mm were heat-treated with the same method (induction heating, vacuum, argon cooling) and applying parameters as in the case of dilatometric tests to ensure the consistency of the results. Since non-proportional samples with a high ratio of the cross-section to the gauge length show an overestimated total elongation (TEl), the uniform elongation (UEl) of the specimen was

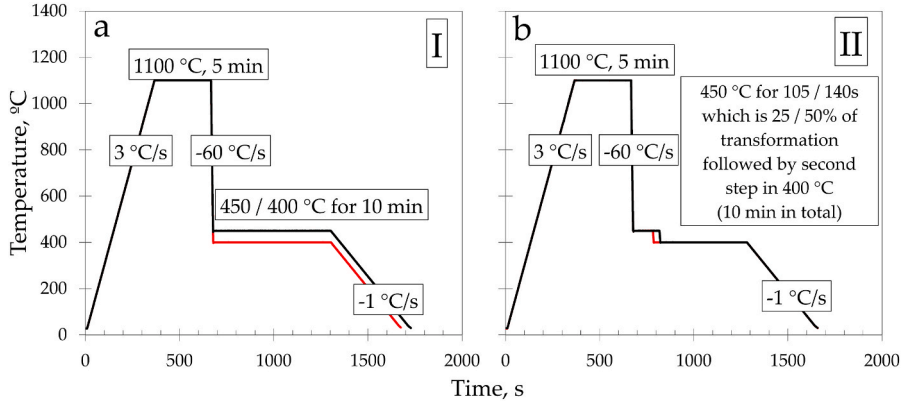

Fig. 2. The types of heat treatment performed for (a) single austempering and (b) double austempering.

used as a determinant of plasticity.

3. Results

3.1. Dilatometric investigations

Fig. 3a presents the cooling curves corresponding to the thermal treatments shown in Fig. 2a. Since M_s is 434 °C, these curves show that part of the austenite has been transformed before starting the austempering step only in the 400C sample. On the contrary, after the bainitic transformation, a part of the remaining austenite is able to transform during cooling to room temperature only in the 450C sample (M_s ~ 83 °C). Fig. 3b shows the relative change in length (RCL) during the isothermal treatment at the two temperatures used. It can be clearly seen that in both cases the bainitic transformation is complete after 10 min. However, some differences are observed between the two curves represented in this figure, consisting of a reduction in both the incubation time and the time required to complete 90% of the transformation (from 32 s to 7 s and from 316 s to 124 s, respectively) in the 400C sample. According to Guo et al. [34], the bainitic reaction is accelerated by the increases of the number of preferential nucleation sites, which are associated with the interfacial energy between preexisting martensite and austenite and the dislocations introduced into the austenite by the formation of martensite, and a larger driving force for the transformation [4,18].

A 10% lower RCL value for the 400C sample in comparison to sample 450C after completion of the bainitic reaction can be observed in Fig. 3b. It has been reported elsewhere that, in general, the RCL value increases when the transformation temperature decreases due to the formation of a larger amount of bainitic ferrite [35]. However, Fig. 3a shows that some part of the austenite was already transformed into martensite before the beginning of the austempering treatment in the 400C sample. Therefore, a smaller fraction of bainite could be formed in this sample than in the 450C sample, and a lower value of the RCL was recorded consequently. The sum of the RLC caused by initial martensitic and subsequent bainitic transformation for sample 400C is ~0.46%. This exceeds the value for the sample 450C (~0.44%), which is in agreement with the literature data [35]. In the first part of the transformation (Fig. 3b, blue arrow), an inhomogeneous transformation is recorded for both samples, which may be associated with microsegregation to which medium manganese steels are susceptible. This phenomenon is highly reduced in the case of sample 400C, where prior martensitic transformation occurred. The issue of microsegregation is addressed in the discussion chapter.

Fig. 3c presents the cooling curves for the two-step austempering treatments shown in Fig. 2b. In this case, no martensitic transformation during cooling was recorded in any of the treatment stages. This indicates that martensitic transformation was prevented for both samples by an increase of the carbon content of the RA during the austempering steps. A slightly higher total RCL for the 25dbl than for 50dbl samples (0.51 and 0.47, respectively) was recorded, as observed in Fig. 3d. The differences in RCL values included in Fig. 3d, indicate that more bainite has been formed for the two-step austempering treatments than in a single step process at 450 °C due to the lower temperature used for the second step, which is in agreement with the results reported in the literature [35]. The sum of RCL related to martensitic and bainitic transformation for sample 400C is lower than the values for double austempered samples. However, it can be explained by the martensite tempering process in sample 400C, which takes place during the isothermal holding step. The carbide precipitation leads to slight sample contraction and a decrease in its total RCL value [36].

3.2. Microstructural characterization

Dilatometric results have been correlated with the microstructure developed after the thermal treatments. Fig. 4 presents OM micrographs for the 450C, 400C and 50dbl samples after etching with Klemm's reagent. This etching solution colors fresh and tempered martensite and bainite, but not cementite or retained austenite. As shown in Fig. 4a, the microstructure of the 450C sample contains blue-colored needles of bainitic ferrite as major constituent, shiny white islands (blocky-type) and films of RA, and a minor amount of brown isolated islands of untempered – fresh martensite.

According to its dilatometric curve, the 400C sample should include tempered martensite and retained austenite together with bainitic ferrite. Since the amount of carbon in solution in bainite and tempered martensite is similar, the color developed by these two phases varies only slightly. In this case, these two phases were identified considering

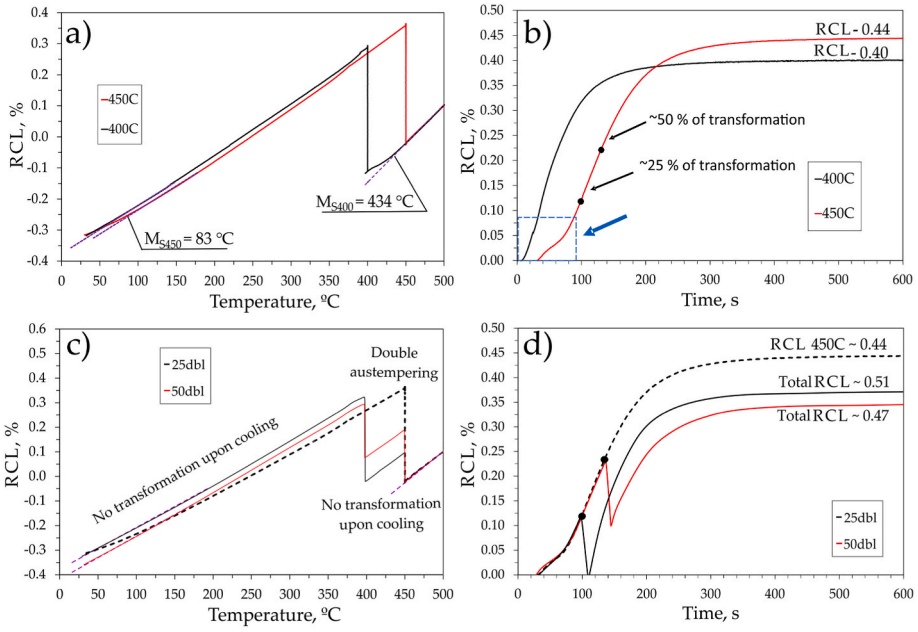

Fig. 3. The dilatometric curves of samples 450C and 400C: (a) cooling; (b) austempering; and samples 25dbl and 50dbl: (c) cooling; (d) double austempering; C-RCL - corrected relative change in length; dashed lines in (c) and (d) represent results for the 450C sample.

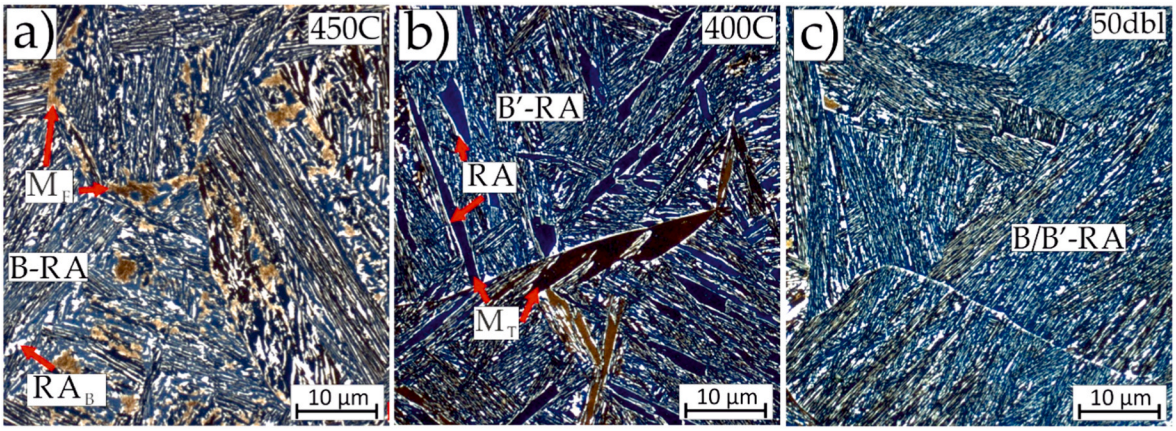

Fig. 4. LM images of samples (a) 450C; (b) 400C; and (c) 50dbl after Klemm's etching; B-RA – bainitic – austenitic regions; B' – refined bainite; M_T – tempered martensite; M_F – fresh martensite; RA_B – blocky type retained austenite.

the differences in size and shape between the colored microstructural constituents. As shown in Fig. 4b, sample 400C presents thin units of acicular shape that are aligned parallel with each other along with bigger elongated features with lath-shaped morphology, which correspond to bainitic ferrite and tempered martensite, respectively. According to image analysis of few regions, the fraction of tempered martensite amounts ~11%. It can also be seen that the RA fraction of blocky morphology has been significantly reduced compared to the 450C sample.

Finally, the microstructure presents after double step austempering (Fig. 4c) only included a mixture of bainitic ferrite and retained austenite mainly of film-like morphology. As shown in Fig. 4c for the 50dbl sample the biggest differences between this microstructure and the previous ones are a lack of fresh/tempered martensite and the presence of two colonies of bainitic sheaves characterized by different average plate thicknesses; the thickest ones formed at 450 °C while the

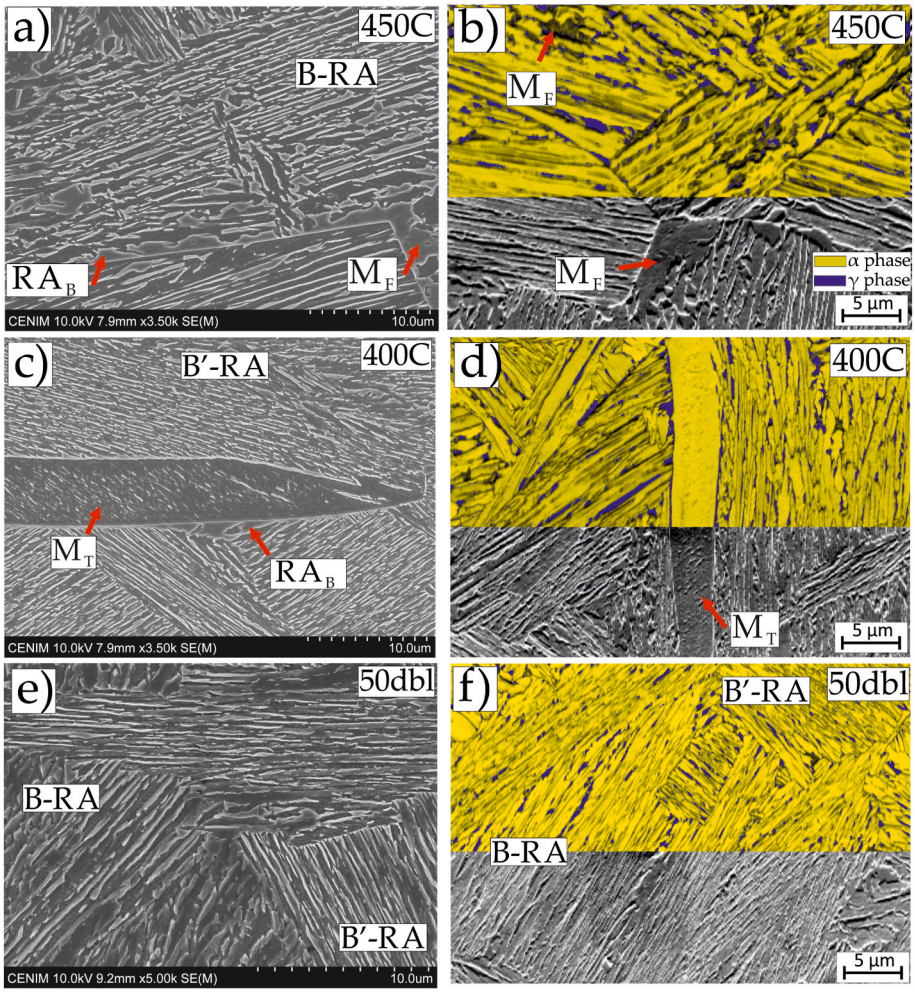

Fig. 5. SEM images (a, c, e) and EBSD maps (b, d, f) of samples 450C, 400C and 50dbl, respectively.

thinnest ones formed during the second step at 400 °C.

Fig. 5 shows the SEM micrographs and the gray-scale image quality map combined with the phase map of the 450C, 400C and 50dbl samples. In the images constructed from the EBSD data, the austenite phase appears in blue, bainite and tempered martensite are in yellow, whereas darker areas indicate poor quality patterns, which were identified as martensite in Fig. 5b for the 450C sample. Although EBSD analysis was very useful to distinguish between martensite and ferrite considering the high dislocation density of martensite, this technique is not capable of resolving austenite films with dimensions smaller than 50–70 nm. As the austenite films present in the samples shown in Fig. 5b, d, and f are much smaller (Fig. 6), neighboring bainite sheaves may produce interference of their diffraction patterns leading to low IQ at these points, and almost only blocky austenite can be seen in these figures. A large discrepancy between the austenite volume fractions measured by EBSD versus XRD was found since the larger amount of retained austenite has a film morphology in these samples.

The 400C sample contains lath-shaped structures with boundaries of wavy shape and ledge-like protrusion. These features correspond to a martensitic structure formed during cooling to 400 °C. As the solubility of carbon at this temperature is very small in the quenched-in martensite, carbon will leave the martensite during the isothermal treatment and carbides will precipitate. As seen in Fig. 5c, tempered martensite includes an abundant presence of nanosized carbides. On the other hand, Fig. 5d show a thin retained austenite layer at the tempered martensite boundary. Kwiatkowski da Silva et al. [37] have reported that both carbon and Mn segregate to dislocations and grain boundaries during tempering of a medium-Mn steel at 450 °C. Thus, during the isothermal holding at 400 °C, the martensite phase boundaries will be enriched in C and Mn, promoting retention of RA films.

Comparing the microstructures presented in Fig. 5, it was again verified that the reduction of the bainitic transformation temperature leads to a reduction in the thickness of the structural components. The clear decrease in the thickness of bainite is visible with an increasing fraction of the low-temperature bainite. The plate thickness distribution diagrams visible in Fig. 6 indicate the clear peaks for bainite formed at both temperatures. As the EBSD method was not capable of resolving thin austenite films, their thickness was measured using high resolution SEM images. Between the samples austempered at 450 °C and 400 °C there is ~25% reduction of average plate thickness. In samples 25dbl (188 nm) and 50dbl (205 nm) in relation to the 450C sample (235 nm) the BPT is reduced by 20% and 14%, respectively. The distribution of film-like RA thickness shows evident domination of RA formed at the lower temperature. The reduction in mean film thickness compared to the 450C sample is 38, 42 and 53% for the samples 50dbl, 25dbl and 400C, respectively. The wide distribution of F-RAT for the 450C sample (much different from the remaining samples) indicates the formation of austenite of very various thicknesses in the later stages of the bainite transformation at higher temperature.

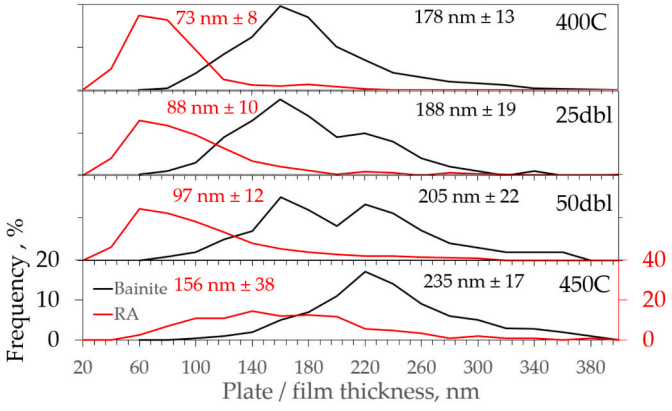

Fig. 6. Apparent bainite plate (BPT) and film-like retained austenite (F-RAT) thickness distribution changes with increasing proportion of refined bainite; the mean values are also indicated. The measurements only included regular film-like RA; blocky-like RA whereas films surrounding the tempered martensite grains were not taken into account.

The theoretical average thickness of the bainite after double tempering, $\overline{L}_{Tdbl}$, has been calculated using a simplified formula that considers the average value of the thicknesses measured in the 450C and 400C samples, $\overline{L}_{T1}$ and $\overline{L}_{T2}$, respectively:

$$\overline{L}_{Tdbl} \sim \%_{T1} \times \overline{L}_{T1} + \%_{T2} \times \overline{L}_{T2} \quad (3)$$

The calculated thickness of bainitic plates for samples 25dbl and 50dbl are 192 and 206 nm, which is in good agreement with experimental results shown in Fig. 6.

The frequency distributions of misorientations angles obtained for the bainitic ferrite in the 450C, 400C and 50dbl samples are very similar, as shown in Fig. 7. As the bainitic ferrite microstructure includes packets of parallel ferritic laths with slight relative misorientations, the peak below 7° was associated with the bainitic ferrite lath boundaries. While the proportion of low-angle boundaries found in the 400C and 50dbl samples is almost the same, a higher proportion for the 450C sample was observed. It is a consequence of an additional influence of fresh martensite nucleated within the austenite during cooling to room temperature. The fresh martensite generates strain and thus increases dislocation density, which rises a fraction of low angle misorientation as reported elsewhere [38]. Fine parallel bainitic ferrite plates with small misorientation are grouped in packets. These packets are mostly separated by high angle boundaries with misorientations ranging between 50 and 65°, which is related to the Kurdjumov-Sachs orientation relationship with the parent austenite grain from which they have nucleated [39]. The increased number of boundaries observed in this range for the 400C and 50dbl samples is thought to be due to the lower temperature used to complete the bainitic reaction, since lower isothermal temperature led to structural refinement and to smaller bainite packets. Beside

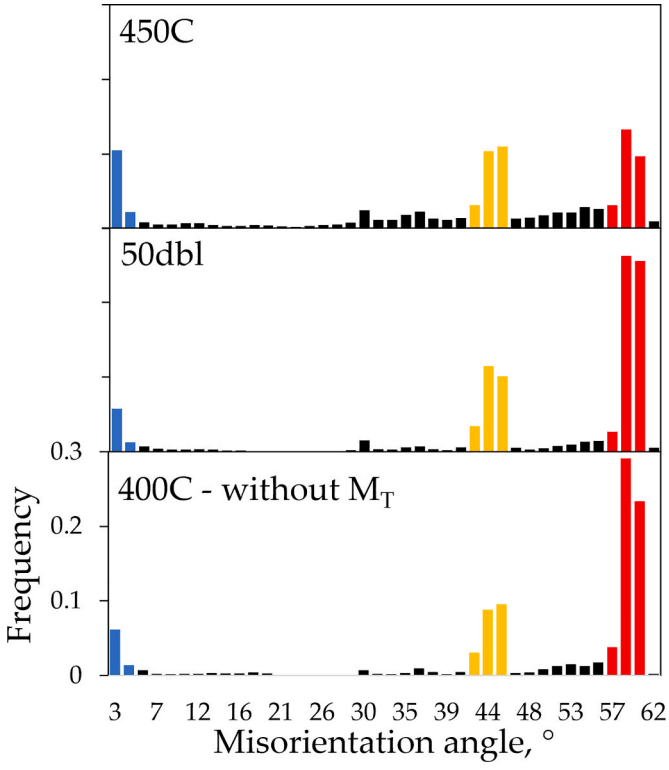

Fig. 7. Changes of misorientation angle between grains with increasing proportion of refined bainite.

these two peaks, it can be seen also in Fig. 7 that the presence of another peak corresponding to grains delimited by ~45° boundaries. Verbeken et al. [40] reported that these angles correspond to the α/γ boundaries. In all samples the frequency of such misorientation related to the retained austenite occurrence is similar.

The values of the RA fraction present in the four samples analyzed and its carbon content are shown in Table 1. As pointed out before, it can be observed a large discrepancy with values reported in this table and the low area fraction observed in the EBSD maps of Fig. 5 because of the limited resolution of EBSD. Although all samples included more than 10% of RA, almost only austenitic grains of blocky morphology present in the 450C sample were detected on the phase maps.

EBSD was almost unable to detect most of the retained austenite with film morphology present in these four samples. However, the combination of image quality (IQ) and phase maps allowed obtaining detailed information on the amount, location, and distribution of the fresh martensite formed during cooling to room temperature. Considering these maps and Table 1, it was concluded that a lower content of C present in the retained austenite of the 450C sample makes it possible to form 6% of fresh martensite during cooling to room temperature. On the other hand, the absence of fresh martensite (<1%) in the 400C, 25dbl and 50dbl samples deduced from the EBSD results, was related to the higher carbon content and film-like of RA in these samples (~1.20 wt%). Although the carbon content is similar in these three samples, the volume fractions of retained austenite do not show a clear dependence with the use of single- or two-step heat treatments as it is affected by the tempering process occurring in the 400C sample.

3.3. Mechanical behavior

Fig. 8 presents the tensile curves of all samples investigated. The key values are summarized in Fig. 9c and correlated with the microstructure features (Fig. 9a) of corresponding samples. The ultimate tensile strength (UTS) of all samples is quite similar – it changes from 1060 MPa for the sample 450C to 1120 MPa for the sample 400C. UTS increases slightly with an increasing fraction of low temperature bainite. The significant difference is visible in a yield strength (YS) level. The sample austempered at 450 °C exhibits the lowest YS of 780 MPa. With increasing the fraction of low temperature bainite the YS value rises up to 960 MPa for sample 25dbl. However, for sample 400 C, the YS is only 830 MPa.

Similar relation as in YS occurs in hardness results which are presented in Fig. 9b. The hardness increases from 323 HV10 to 377 HV10 for samples 450C and 25dbl, respectively. However, its value is lower in case of sample 400C (354 HV10). The increase in strength and hardness of the material is generally related to the microstructure refinement, especially the reduction of the bainitic plates thickness [1]. Sample 400C despite the most refined bainite and austenite, contains also some fraction of coarse tempered martensite, which weakens the microstructure [4,18]. Sample 450C exhibits the ultimate elongation (UEl) of 13%, despite the presence of globular fresh martensite in the microstructure, which is the highest value among all samples. It is caused by the coarser microstructure, lower YS, and relatively high proportion of RA. The sample 400C contains a similar fraction of this phase – which is mostly responsible for plastic properties. However, sample 400C exhibits lower plasticity (UEl – 11%) due to tempered martensite and more refined microstructure. The double treated samples exhibit the highest YS. However, it is at the price of lowest UEl of ~9%, which is caused by very fine microstructure and a lower RA fraction.

Table 1
Quantitative evaluation of microstructure: RA fraction; C concentration in RA; fresh and tempered martensite fraction for microstructures with different heat treatment.

Sample	RA, % EBSD	RA, % XRD	x_C, wt, % (±0.12)	M_F, %	M_T, %
450C	10.4 ± 1.8	14.7 ± 2	1.08	6.1 ± 0.8	–
50dbl	6.7 ± 1.0	13.3 ± 2	1.20	<1	–
25dbl	6.5 ± 1.1	10.0 ± 2	1.21	<1	–
400C	7.2 ± 1.2	14.3 ± 2	1.22	<1	11 ± 3

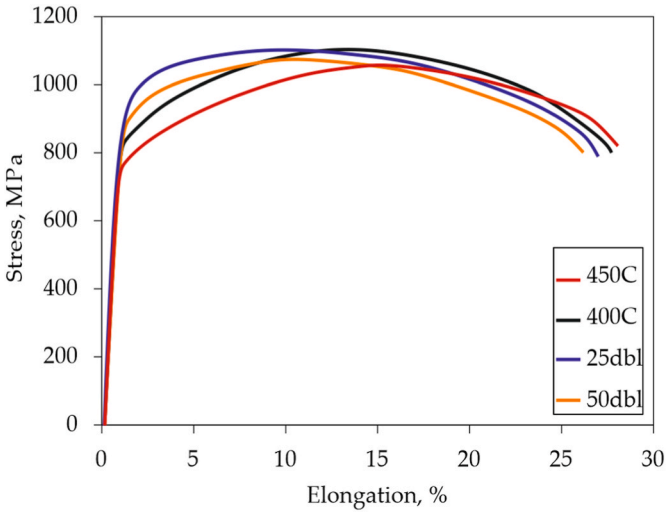

Fig. 8. Uniaxial tensile test results for investigated heat treatments.

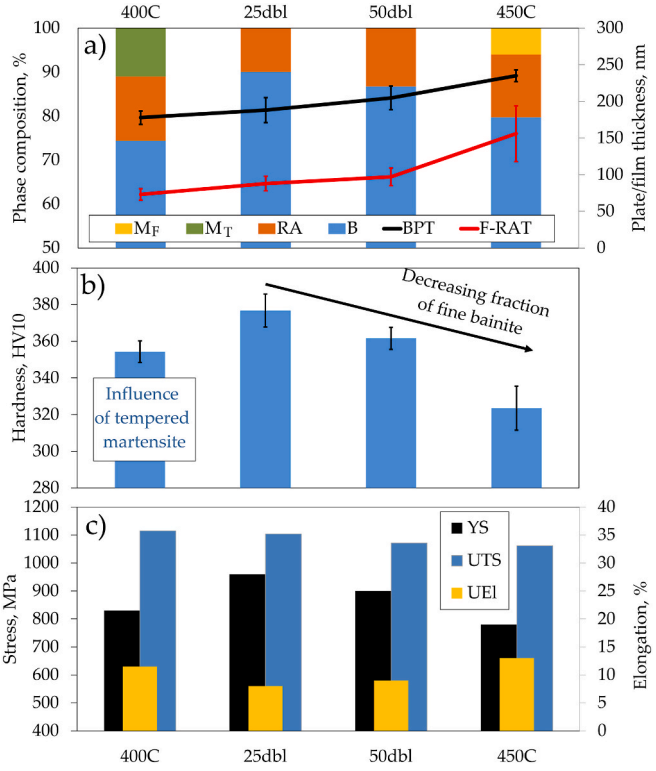

Fig. 9. Mechanical properties change accompanying the microstructural changes; (a) phase composition and thickness of microstructural constituents; (b) hardness; (c) summarized tensile test results.

4. Discussion

4.1. Transformation kinetics and microsegregation

Despite the increased addition of manganese in steel, which significantly delays the bainitic transformation [35,45,46], in all cases it is completed below 10 min. This is due to the large addition of Al in the

steel (1.6 wt%). Al in bainitic TRIP-aided steels is basically added to reduce the harmful effect of carbides on RA stabilization [5,47]. However, Al is also a strong α phase stabilizer, which increases the driving force for bainitic transformation and therefore accelerates the transformation time itself [48,49]. The tested steel, despite the increased content of manganese, balances its slowing effect on the bainitic transformation with the addition of aluminum, which allows for a significant reduction in heat treatment time. The obvious advantages of medium-Mn steels in terms of RA stabilization, however, may be associated with some problems - microsegregation, to which these steels are susceptible [41,42]: (i) grain boundary segregation and (ii) segregation banding [41]. The areas containing a lower content of Mn undergo the transformation faster due to the increased kinetics compared to the alloy with a bulk chemical composition [43]).

The dilatometric curves of the austempered steels indicate such an inhomogeneous transformation (Fig. 3b). Some areas of the sample undergo transformation faster than others, which is illustrated by a distorted shape of the curve. This phenomenon is confirmed by its high reduction in the case of sample 400C, which indicates that the areas less enriched in chemical elements undergo the transformation as first – during initial martensitic transformation. Previous tests of analyzed steel at the casting and forging stage confirmed the presence of microsegregation [44,45], which has been significantly limited by soaking and thermomechanical processing (forging and hot rolling). However, the current results confirm that it has not been completely eliminated.

The influence of microsegregation on the transformation kinetics is also clearly visible in the results of M_s at different degrees of bainitic transformation. The decrease in M_s temperature (Fig. 1) is the strongest in the first 10% of the bainite transformation (~44 °C). Usually, stronger stabilization is expected to occur in the late or final stage of the transformation, where the distances between the adjacent sheaves of bainite shorten the diffusion path through the fragmentation of the post-austenite and the greater carbon enrichment of the austenite. Close-up of the quenching curve (Fig. 10) shows that the martensitic transformation of the tested material does not start globally (which would be represented by a sudden increase in elongation [46]) but gradually. In the first stage, austenitic areas with a lower manganese content, which are less stable, undergo transformation. This relationship allows for a significant reduction in M_s of the remaining part of austenite with a small degree of bainite transformation. This can be a way to improve the strength properties of steels exposed to the microsegregation phenomenon.

To investigate the effect of microsegregation on the microstructure, samples quenched after 25 (25Q) and 50% (50Q) of bainitic transformation were used to investigate the evolution of bainitic transformation. LM images covering 1000 × 700 μm illustrate the mechanism

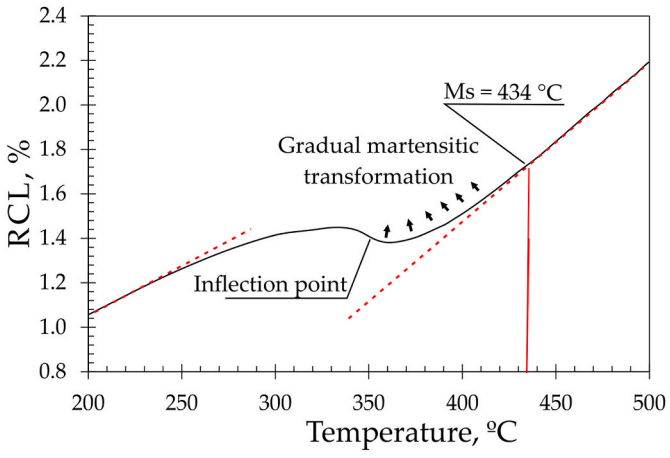

Fig. 10. The cooling curve of the quenched sample presenting the influence of microsegregation on martensitic transformation kinetics.

of nucleation and growth of bainite (Fig. 11).

Both microstructures are composed of RA-B islands (bright blue), and martensite (brown and navy blue) formed at high-temperature (M_H). The nucleation of bainite seems to be homogeneous. Single regions poorer in bainite relative to the rest of the microstructure can be indicated (yellow ellipses). However, it may also be the result of the stochastic nature of bainite nucleation [1], as it is highly limited compared to the typical distribution of solute at the dendritic scale [47]. No privileged nucleation regions that may be associated with macrosegregation (bands) [42] were observed.

4.2. Evolution of bainitic transformation

It is interesting that 450C sample (Fig. 4a) exhibits a relatively high fraction of blocky-type RA and martensite, while in sample 25dbl and even 50dbl (Fig. 4c) it is strongly limited. The observations show that in the first stage of bainitic transformation (Fig. 11a), single sheaves consisting of a small number of connected bainite plates grow into the grain. Even after 50% of the bainitic transformation at 450 °C (Fig. 11b), the vast majority of the boundary of bainite sheaves is constituted by high-temperature martensite (former austenite). This means that the period of privileged formation of blocky-type RA grains at the boundaries of nonparallel bainitic sheaves occurs in the second half of transformation, when "gaps" in the bainitic + film-like RA microstructure are filled. It is also visible in the initial dilatometric results (Fig. 1). The M_s of high-temperature martensite decreases with the progress of the bainitic transformation (342 °C after 90%), and the martensitic transformation becomes less intense. The first is related to the slight stabilization of RA and the second is related to the decreasing fraction of high-temperature austenite. For 100% of possible bainite transformation at 450 °C, the martensitic transformation of high-temperature austenite does not occur, while the cooling curve records sample elongation corresponding to transformation of blocky type RA at ~83 °C (Fig. 3), what was revealed by microscopic observations (Figs. 4 and 5).

Fig. 12 presents the characteristic with progress of the bainitic transformation at 450 °C. It combines the results from samples quenched after 25% (25Q) and 50% (50Q) of bainitic transformation and after its completion (450C). The overall fraction of RA in the microstructure increases during transformation (Fig. 12a). The strongest increase is visible in the first 50% (increase of ~10%) of transformation. Later, this value grows only by 4.6%. However, it should be noted that the microstructure of 450C sample contains ~6% of fresh martensite. Hence, it can be assumed that the total fraction of austenite immediately after bainitic transformation at 450 °C was ~20%. The amount of fresh martensite in the sample 50dbl is negligible (Table 1), which confirms earlier theory about period of blocky-type RA formation (Fig. 12a). It is reflected also in the average carbon concentration in austenite, which very slightly decreases with transformation (from 1.12 to 1.08%). The proportion of blocky, low-enriched RA grows with time of transformation, affecting the average concentration value. Second factor influencing C concentration may be the average RA film thickness, which rises significantly with progress of the transformation, as evidenced by performed measurements (Fig. 12b). This increase results in a smaller proportion of the adjacent bainite per volume unit of austenite and thus its lower possible carbon enrichment.

Changes in RA size is probably related to the increasing thickness of bainite. It grows continuously (Fig. 12b) with a progress of transformation from 212 nm after 25% up to 235 nm after the transformation completion. This phenomenon is consistent with the literature [48] and is caused by the changes in the yield strength of the austenite from which the bainite grows and the decrease in transformation rate (driving force for transformation) as transformation proceeds. Hardness decreases with a progress of transformation, which is obviously caused by a decrease in high temperature martensite fraction (Figs. 11 and 12).

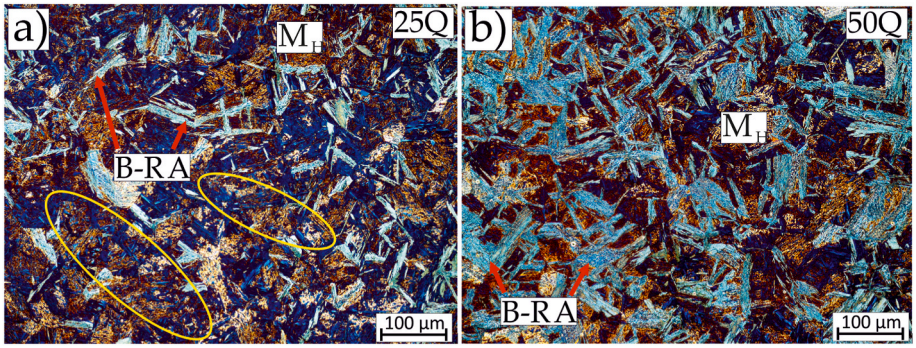

Fig. 11. LM images (Klemm's etching) of samples (a) 25Q and (b) 50Q; M_H – high temperature martensite; B-RA – bainitic – austenitic regions; red ellipses indicate places with a reduced number of bainite plates. (For interpretation of the references to color in this figure legend, the reader is referred to the Web version of this article.)

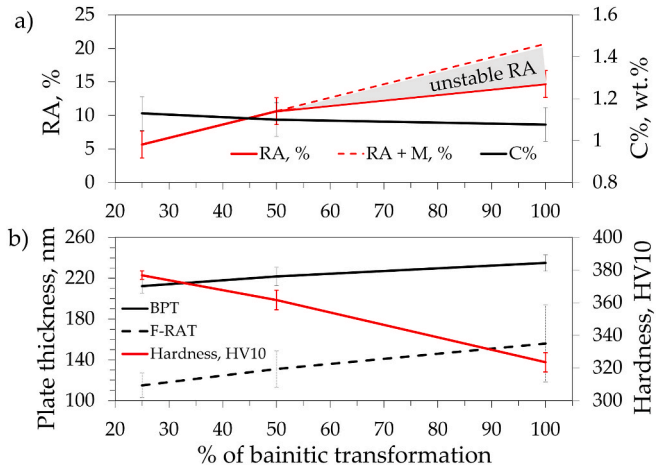

Fig. 12. Evolution of the microstructure with the progress of bainitic transformation at 450 °C; (a) fraction of RA and martensite and corresponding carbon concentration in RA; (b) evolution of hardness and thickness of bainite (BPT) and film-like retained austenite (F-RAT).

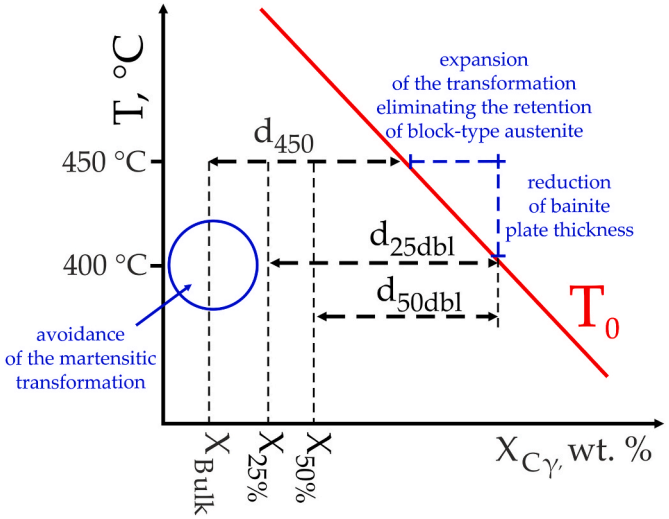

Fig. 13. The application of the T_0 rule in the case of double austempering; d_x – fraction of bainite that can be formed.

4.3. Double austempering

All phenomena occurring in double austempering may be explained by T_0 rule (Fig. 13). The T_0 line limits the possible bainite fraction formed [1]. At 450 °C after transformation completion there are still coarse regions (Fig. 4a) of austenite in the microstructure which are too much enriched in C to undergo further bainitic transformation (crossed T_0 line). However, they are not sufficiently stabilized to maintain the stability to room temperature, which results in martensitic transformation during cooling and weakening of the microstructure. The reduction of temperature to 400 °C expands the allowable carbon content in austenite, which may transform into bainite, promoting extended transformation and thus RCL of the sample (Fig. 3d) (in case of sample 400C limited by prior martensitic transformation). In case of double austempered samples both favorable mechanisms are combined. First transformation is performed at a temperature not threatened by the martensitic transformation, which allows to stabilize remaining austenite slightly (represented by M_s temperature reduction visible in Fig. 1). After the following temperature reduction, the bainitic transformation is completed in the extended way, which besides reduction of the film-like RA and bainitic plate thickness allows for transformation of pre-enriched austenitic regions [2,3]. It strongly reduces the possibility of retaining of blocky-type RA and thus possible fresh martensite formation [49]. The lack of brittle fresh or coarse tempered martensite in the microstructure improves its homogeneity and thus the mechanical properties of the steel [8]. The difference between UTS and YS depends on the RA fraction. This phase is responsible for the strain hardening. Therefore, in sample 450C despite the lowest YS, the UTS reached almost the level of sample 25dbl as the microstructure exhibits a higher fraction of low stable RA. It is interesting that the hardness of sample containing 50% high temperature martensite (380 HV10) is at the same level as sample 25dbl (377 HV10), composed in >75% of refined bainite. It shows that the reduction of the bainite plate thickness has a great impact on the overall properties of the alloy [8,21].

5. Conclusions

The following conclusions were drawn from the detailed study performed on the 3.3Mn-0.17C-1.6Al-0.23Mo-0.22Si multiphase steel to investigate the microstructure-properties evolution:

- The reduction of the bainite transformation temperature below the M_s (from 450 to 400 °C) allows to obtain a multiphase microstructure, which is characterized by a decrease in the thickness of both the bainite plate and film-type retained austenite (25% and 53%, respectively). After this treatment the hardness increased by 31 HV, YS by 50 MPa, and a significant reduction of the amount of both blocky-type RA and brittle fresh martensite was obtained but at the

cost of producing of a certain amount of tempered martensite in the microstructure.

- The implementation of double austempering treatment consisting of austempering at 450 °C up to 25 and 50% transformation, followed by an isothermal treatment at 400 °C to complete the reaction, allowed almost entire removal of tempered martensite and blocky RA. Starting the transformation at a higher temperature also allowed for the elimination of tempered martensite in the microstructure.
- The reduction in thickness of the bainite plate and the film-type retained austenite reached by double-austempering treatment is somewhat lower than that achieved in the isothermal treatment at 400 °C (about 20–14 and 42-38%, respectively). However, the additional increase of the hardness (8 and 23 HV) and YS (70 and 130 MPa) while maintaining over 8% of UEl associated to the microstructural refinement and absence of tempered martensite occurred.
- The privileged formation of blocky-type RA in the second half of bainitic transformation at 450 °C was evidenced. Both bainite plate and film-like austenite thickness increases with bainitic transformation progress.
- The increased content of Mn slows down the bainitic transformation kinetics. However, the replacement of Si by Al in the alloy allows counteracting this effect and completing the bainite transformation in less than 10 min.

CRediT authorship contribution statement

Adam Skowronek: Conceptualization, Data curation, Funding acquisition, Investigation, Methodology, Resources, Visualization, Writing – original draft. **Erick Cordova-Tapia:** Data curation, Investigation, Methodology. **Pilar Tobajas-Balsera:** Investigation, Visualization. **Carlos Garcia-Mateo:** Conceptualization, Formal analysis, Methodology, Resources, Software, Supervision, Validation, Writing – review & editing. **José A. Jiménez:** Formal analysis, Investigation, Writing – original draft. **Roumen Petrov:** Methodology, Resources, Software. **Adam Grajcar:** Conceptualization, Formal analysis, Project administration, Supervision, Validation, Writing – review & editing.

Declaration of competing interest

The authors declare that they have no known competing financial interests or personal relationships that could have appeared to influence the work reported in this paper.

Data availability

Data will be made available on request.

Acknowledgments

Adam Skowronek is a holder of European Union scholarship through the European Social Fund, grant InterPOWER (POWR.03.05.00–00-Z305).

Publication supported under the Rector's pro-quality grant. Silesian University of Technology, grant no. 10/010/RGJ21/1034.

References

[1] C. Garcia-Mateo, F. Caballero, H. Bhadeshia, Development of hard bainite, ISIJ Int. 43 (2003), https://doi.org/10.2355/isijinternational.43.1238.
[2] C. Garcia-Mateo, G. Paul, M. Somani, D. Porter, L. Bracke, A. Latz, C. Garcia De Andres, F. Caballero, Transferring nanoscale bainite concept to lower C contents: a perspective, Metals 7 (2017) 159, https://doi.org/10.3390/met7050159.
[3] J. Cornide, C. Garcia-Mateo, C. Capdevila, F.G. Caballero, An assessment of the contributing factors to the nanoscale structural refinement of advanced bainitic steels, Alloys Compd. 577 (2013) S43–S47, https://doi.org/10.1016/j.jallcom.2011.11.066.
[4] J. Tian, G. Xu, M. Zhou, H. Hu, Refined bainite microstructure and mechanical properties of a high-strength low-carbon bainitic steel treated by austempering below and above Ms, Steel Res. Int. 89 (2018) 1700469, https://doi.org/10.1002/srin.201700469.
[5] J. Yang, T.S. Wang, B. Zhang, F.C. Zhang, Microstructure and mechanical properties of high-carbon Si–Al-rich steel by low-temperature austempering, Mater. Des. 35 (2012) 170–174, https://doi.org/10.1016/j.matdes.2011.08.041.
[6] F.G. Caballero, H.K.D.H. Bhadeshia, K.J.A. Mawella, D.G. Jones, P. Brown, Very strong low temperature bainite, Mater. Sci. Technol. 18 (2002) 279–284, https://doi.org/10.1179/026708301225000725.
[7] H.K.D.H. Bhadeshia, Bulk nanocrystalline steel, Ironmak. Steelmak. 32 (2005) 405–410, https://doi.org/10.1179/174328105X71308.
[8] X.L. Wang, K.M. Wu, F. Hu, L. Yu, X.L. Wan, Multi-step isothermal bainitic transformation in medium-carbon steel, Scripta Mater. 74 (2014) 56–59, https://doi.org/10.1016/j.scriptamat.2013.10.019.
[9] T. Sourmail, C. Garcia-Mateo, F.G. Caballero, L. Morales-Rivas, R. Rementeria, M. Kuntz, Tensile ductility of nanostructured bainitic steels: influence of retained austenite stability, Metals 7 (2017) 31, https://doi.org/10.3390/met7010031.
[10] C. Garcia-Mateo, F. Caballero, The role of retained austenite on tensile properties of steels with bainitic microstructures,, Mater. Trans. 46 (2005), https://doi.org/10.2320/matertrans.46.1839.
[11] E. Bonnevie, G. Ferrière, A. Ikhlef, D. Kaplan, J.M. Orain, Morphological aspects of martensite–austenite constituents in intercritical and coarse grain heat affected zones of structural steels, Mater. Sci. Eng. A 385 (2004) 352–358, https://doi.org/10.1016/j.msea.2004.06.033.
[12] K. Sugimoto, J. Sakaguchi, T. Iida, T. Kashima, Stretch-flangeability of a high-strength TRIP type bainitic sheet steel, ISIJ Int. 40 (2000) 920–926, https://doi.org/10.2355/isijinternational.40.920.
[13] K. Hase, C. Garcia-Mateo, H.K.D.H. Bhadeshia, Bimodal size-distribution of bainite plates, Mater. Sci. Eng. A (2006) 145–148, https://doi.org/10.1016/j.msea.2005.12.070, 438-440.
[14] C. Garcia-Mateo, F.G. Caballero, J. Chao, C. Capdevila, C. Garcia de Andres, Mechanical stability of retained austenite during plastic deformation of super high strength carbide free bainitic steels, Mater. Sci. 44 (2009) 4617–4624, https://doi.org/10.1007/s10853-009-3704-4.
[15] K.-W. Kim, K. Il Kim, C.-H. Lee, J.-Y. Kang, T.-H. Lee, K.-M. Cho, K.H. Oh, Control of retained austenite morphology through double bainitic transformation, Mater. Sci. Eng. A 673 (2016) 557–561, https://doi.org/10.1016/j.msea.2016.07.083.
[16] I. Yakubtsov, G. Purdy, Analyses of transformation kinetics of carbide-free bainite above and below the athermal martensite-start temperature, Metall. Mater. Trans. A 43 (2011), https://doi.org/10.1007/s11661-011-0911-9.
[17] S. Samanta, P. Biswas, S. Giri, S. Singh, S. Kundu, Formation of bainite below the M S temperature: kinetics and crystallography, Acta Mater. 105 (2016) 390–403, https://doi.org/10.1016/j.actamat.2015.12.027.
[18] J. Tian, G. Xu, Z. Jiang, Q. Yuan, G. Chen, H. Hu, Effect of austenisation temperature on bainite transformation below martensite starting temperature, Mater. Sci. Technol. 35 (2019) 1–12, https://doi.org/10.1080/02670836.2019.1631946.
[19] M. Soliman, H. Mostafa, A.S. El-Sabbagh, H. Palkowski, Low temperature bainite in steel with 0.26wt% C, Mater. Sci. Eng. A 527 (2010) 7706–7713, https://doi.org/10.1016/j.msea.2010.08.037.
[20] H. Mousalou, S. Yazdani, B. Avishan, N.P. Ahmadi, A. Chabok, Y. Pei, Microstructural and mechanical properties of low-carbon ultra-fine bainitic steel produced by multi-step austempering process, Mater. Sci. Eng. A 734 (2018) 329–337, https://doi.org/10.1016/j.msea.2018.08.008.
[21] V.T. Duong, Y.Y. Song, K.-S. Park, H.K.D.H. Bhadeshia, D.-W. Suh, Austenite in transformation-induced plasticity steel subjected to multiple isothermal heat treatments, Metall. Mater. Trans. A 45 (2014) 4201–4209, https://doi.org/10.1007/s11661-014-2405-z.
[22] B. Avishan, M. Tavakolian, S. Yazdani, Two-step austempering of high performance steel with nanoscale microstructure, Mater. Sci. Eng. A 693 (2017) 178–185, https://doi.org/10.1016/j.msea.2017.03.104.
[23] A. El-Sherbiny, M.K. El-Fawkhry, A.Y. Shash, T. El-Hossany, Replacement of silicon by aluminum with the aid of vanadium for galvanized TRIP steel, Mater. Res. Technol. 9 (2020) 3578–3589, https://doi.org/10.1016/j.jmrt.2020.01.096.
[24] H. Bin, L. Haiwen, Y. Feng, D. Han, Recent progress in medium-Mn steels made with new designing strategies, a review, Mater. Sci. Technol. 44 (2017) 1457–1464.
[25] J. Chiang, J.D. Boyd, A.K. Pilkey, Effect of microstructure on retained austenite stability and tensile behaviour in an aluminum-alloyed TRIP steel, Mater. Sci. Eng. A 638 (2015) 132–142, https://doi.org/10.1016/j.msea.2015.03.069.
[26] Astm A1033-04, Standard practice for quantitative measurement and reporting of hypoeutectoid carbon and low-alloy steel phase transformations; ASTM International: west Conshohocken. https://www.astm.org/, 2004 accessed July 25, 2020.
[27] H.-S. Yang, H.K.D.H. Bhadeshia, Uncertainties in dilatometric determination of martensite start temperature, Mater. Sci. Technol. 23 (2007) 556–560, https://doi.org/10.1179/174328407X176857.
[28] N. van Dijk, A. Butt, L. Zhao, J. Sietsma, S. Offerman, J. Wright, S. Zwaag, Thermal stability of retained austenite in TRIP steels studied by synchrotron X-ray diffraction during cooling, Acta Mater. 53 (2005) 5439–5447, https://doi.org/10.1016/j.actamat.2005.08.017.
[29] R. Petrov, L. Kestens, A. Wasilkowska, Y. Houbaert, Microstructure and texture of a lightly deformed TRIP-assisted steel characterized by means of the EBSD technique, Mater. Sci. Eng., A 447 (2007) 285–297, https://doi.org/10.1016/j.msea.2006.10.023.

[30] J. Wu, P.J. Wray, C.I. Garcia, M. Hua, A.J. Deardo, Image quality analysis: a new method of characterizing microstructures, ISIJ Int. 45 (2005) 254–262, https://doi.org/10.2355/isijinternational.45.254.
[31] M.J. Santofimia, R.H. Petrov, L. Zhao, J. Sietsma, Microstructural analysis of martensite constituents in quenching and partitioning steels, Mater. Char. 92 (2014) 91–95, https://doi.org/10.1016/j.matchar.2014.03.003.
[32] C. Garcia-Mateo, J.A. Jimenez, B. Lopez-Ezquerra, R. Rementeria, L. Morales-Rivas, M. Kuntz, F.G. Caballero, Analyzing the scale of the bainitic ferrite plates by XRD, SEM and TEM, Mater. Char. 122 (2016) 83–89, https://doi.org/10.1016/j.matchar.2016.10.023.
[33] L.C. Chang, H.K.D.H. Bhadeshia, Austenite films in bainitic microstructures, Mater. Sci. Technol. 11 (1995) 874–882, https://doi.org/10.1179/mst.1995.11.9.874.
[34] H. Guo, X. Feng, A. Zhao, Q. Li, J. Ma, Influence of prior martensite on bainite transformation, microstructures, and mechanical properties in ultra-fine bainitic steel, Materials 12 (2019) 527, https://doi.org/10.3390/ma12030527.
[35] H.K.D.H. Bhadeshia, J.W. Christian, Bainite in steels, Metall. Mater. Trans. A 21 (1990) 767–797, https://doi.org/10.1007/BF02656561.
[36] A. Navarro-López, J. Sietsma, M.J. Santofimia, Effect of prior athermal martensite on the isothermal transformation kinetics below Ms in a low-C high-Si steel, Metall. Mater. Trans. A 47 (2016) 1028–1039, https://doi.org/10.1007/s11661-015-3285-6.
[37] A. Kwiatkowski da Silva, G. Inden, A. Kumar, D. Ponge, B. Gault, D. Raabe, Competition between formation of carbides and reversed austenite during tempering of a medium-manganese steel studied by thermodynamic-kinetic simulations and atom probe tomography, Acta Mater. 147 (2018) 165–175, https://doi.org/10.1016/j.actamat.2018.01.022.
[38] N.P. Gurao, S. Suwas, Generalized scaling of misorientation angle distributions at meso-scale in deformed materials, Sci. Rep. 4 (2014) 5641, https://doi.org/10.1038/srep05641.
[39] S.L. Shrestha, A.J. Breen, P. Trimby, G. Proust, S.P. Ringer, J.M. Cairney, An automated method of quantifying ferrite microstructures using electron backscatter diffraction (EBSD) data, Ultramicroscopy 137 (2014) 40–47, https://doi.org/10.1016/j.ultramic.2013.11.003.
[40] K. Verbeken, L. Barbé, D. Raabe, Evaluation of the crystallographic orientation relationships between FCC and BCC Phases in TRIP steels, ISIJ Int. 49 (2009) 1601–1609, https://doi.org/10.2355/isijinternational.49.1601.
[41] J. Hidalgo, C. Celada-Casero, M.J. Santofimia, Fracture mechanisms and microstructure in a medium Mn quenching and partitioning steel exhibiting macrosegregation, Mater. Sci. Eng., A 754 (2019) 766–777, https://doi.org/10.1016/j.msea.2019.03.055.
[42] J. Liang, Z. Zhao, D. Tang, N. Ye, S. Yang, W. Liu, Improved microstructural homogeneity and mechanical property of medium manganese steel with Mn segregation banding by alternating lath matrix, Mater. Sci. Eng. A 711 (2018) 175–181, https://doi.org/10.1016/j.msea.2017.11.046.
[43] M. Morawiec, V. Ruiz-Jimenez, C. Garcia-Mateo, A. Grajcar, Thermodynamic analysis and isothermal bainitic transformation kinetics in lean medium-Mn steels, Therm. Anal. Calorim. 142 (2020) 1709–1719, https://doi.org/10.1007/s10973-020-10259-z.
[44] A. Grajcar, M. Kamińska, M. Opiela, P. Skrzypczyk, B. Grzegorczyk, E. Kalinowska-Ozgowicz, Segregation of alloying elements in thermomechanically rolled medium-Mn multiphase steels, Achiev. Mater. Manuf. 55 (2012) 256–264.
[45] A. Grajcar, Segregation behaviour of third generation advanced high-strength Mn-Al steels, Arch. Foundry Eng. 12 (2012) 123–128, https://doi.org/10.2478/v10266-012-0049-2.
[46] C. García de Andrés, F.G. Caballero, C. Capdevila, L.F. Álvarez, Application of dilatometric analysis to the study of solid–solid phase transformations in steels, Mater. Char. 48 (2002) 101–111, https://doi.org/10.1016/S1044-5803(02)00259-0.
[47] A. Basso, A. Eres-Castellanos, N. Tenaglia, D. San-Martin, J.A. Jimenez, F. G. Caballero, Effect of microsegregation and bainitic reaction temperature on the microstructure and mechanical properties of a high-carbon and high-silicon cast steel, Metals 11 (2021) 220, https://doi.org/10.3390/met11020220.
[48] V. Ruiz-Jimenez, J. JimÉNEZ, F. Caballero, C. Garcia-Mateo, Bainitic ferrite plate thickness evolution in two nanostructured steels, Materials 14 (2021) 4347, https://doi.org/10.3390/ma14154347.
[49] K. Sugimoto, K. Nakano, S.-M. Song, T. Kashima, Retained austenite characteristics and stretch-flangeability of high-strength low-alloy TRIP type bainitic sheet steels, ISIJ Int. 42 (2002) 450–455, https://doi.org/10.2355/isijinternational.42.450.